Real-Time Scanning Charged-Particle Microscope Image Composition with Correction of Drift

Petr Cizmar, András E. Vladár, and Michael T. Postek
National Institute of Standards and Technology, 100 Bureau Drive, Gaithersburg, MD 20899

In this article, a new scanning electron microscopy (SEM) image composition technique is described, which can significantly reduce drift related image corruptions. Drift-distortion commonly causes blur and distortions in the SEM images. Such corruption ordinarily appears when conventional image-acquisition methods, i.e. "slow scan" and "fast scan", are applied. The damage is often very significant; it may render images unusable for metrology applications, especially, where sub-nanometer accuracy is required. The described correction technique works with a large number of quickly taken frames, which are properly aligned and then composed into a single image. Such image contains much less noise than the individual frames, whilst the blur and deformation is minimized. This technique also provides useful information about changes of the sample position in time, which may be applied to investigate the drift properties of the instrument without a need of additional equipment.

INTRODUCTION

Advances in fundamental nano-science, development of nano-materials, and eventually manufacturing of nanometer-scale products all depend to some extent on the capability to accurately and reproducibly measure dimensions, properties, and performance characteristics at the nano-scale. Scanning electron microscopes (SEMs) have been used in this application for many years [8], [9]. Since progress in nano-science and nano-technology has been rather rapid recently, the dimensions of nano-structures and nano-objects have shrunk significantly. Consequently, accurate SEM imaging has been emphasized. The dimensions or distances have been measured from SEM images or line-scans. Current imaging methods in SEM are often incapable of achieving the desired accuracy, because the SEM images, at such high magnifications, often suffer from drift-related distortion. In many cases, the drift is significant and the SEM images exhibit deformations or blur. The same problem is also experienced in other fields, e.g. scanning probe microscopies.

Several correction methods are being developed that compensate for these effects. Some work on correcting the time-dependent drift distortions has been performed in fields similar to scanning electron microscopy [5], [6], [1], [13]. A research in drift-distortion evaluation and correction in SEMs has been published in [12], [11], [10]. Technique described in these papers covers correction in images with slow drift and low magnification. The overall imaging times are high, reaching tens of minutes. The magnification does not exceed 10000. Technique for very fast SEM or Scanning helium-ion beam microscopy, where signal-to-noise ratio (SNR) may drop below 5×10^{-1}, is still needed. This manuscript describes a possible correction method based on composition of drift-distortion corrected SEM images. The technique uses cross-correlation for displacement detection. It not only provides more accurate images, but also sample position information, which can be successfully employed in diagnostic applications. The method is implemented as a software program in the C programming language. With this approach, the solution is fast, multi-platform, multi-processor capable, and moreover can be easily integrated into the majority of the SEM software.

DRIFT EFFECT ON IMAGES

In the SEM, the image is formed by scanning over the sample and acquisition of an intensity value at each location on the sample corresponding to a pixel in the image. The intensity value $\xi(\vec{r})$ depends on the landing position of the electron beam (on the sample) $\vec{r}$. Most SEMs use the raster pattern for scanning over the sample. Let the raster pattern be defined by the time-dependent vector function:

$$\vec{r}_r(t) = M\left(x(t)\vec{e}_x + y(t)\vec{e}_y\right), \tag{1}$$

$$t_p = t_D + t_d,$$

$$y(t) = \left\lfloor \frac{t}{Xt_p + t_j} \right\rfloor, \tag{2}$$

$$x(t) = \left\lfloor \frac{t}{t_p} \right\rfloor - Xy(t), \tag{3}$$

$$0 \le t \le Y(Xt_p + t_j),$$

where t is time, M is a constant of the length on sample corresponding to a single-pixel step. x and y are column and row indexes in the SEM image. $\vec{e_x}$ and $\vec{e_y}$ are the unit vectors in x- and y-direction, t_D is the dwell time of one pixel, t_d is the dead time between two pixels, t_j is the time needed to move the beam to the beginning of the new line. $\lfloor q \rfloor$ is a symbol for the floor(q) function as used in programming languages. X and Y are the pixel-width and pixel-height of the SEM image. These equation are in agreement with those published in [12].

Imaging in the SEM may be defined as a relation between the intensity map of the sample $\xi(\vec{r})$ and the SEM image $I(x, y)$:

$$I(x(t), y(t)) = K\xi(\vec{r}(t)). \tag{4}$$

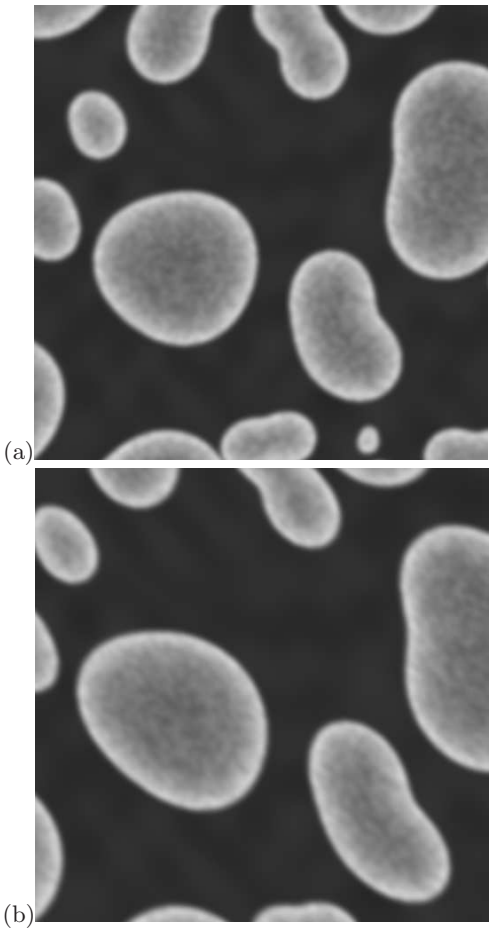

FIG. 1. Illustration of drift-distortion-related image corruption on simulated [2] "slow scan" SEM images of a gold-on-carbon sample. (a) Ideal, undistorted image. (b) Typical corrupted image.

The relation between I and ξ may in practice be very general. For simplicity, let K be a constant in this paper, since this does not affect generality of the described technique. In the ideal case $\vec{r}(t) = \vec{r}_r(t)$; however, drift and space distortions are always present in scanning microscopes and they often significantly affect the position $\vec{r}$:

$$\vec{r}(t) = \vec{r}_r(t) + \vec{D}_d(t) + \vec{D}_s(\vec{r}_r). \tag{5}$$

The space distortion $\vec{D}_s$ is constant in time and may be simply compensated for, when its function is known. This kind of distortion is caused by non-linearities in deflection amplifiers and appears mostly at low magnifications. On the other hand, the drift distortion $\vec{D}_d$ is changing in time, its function is usually unknown, and it most significantly affects the high-magnification images. The drift distortion may arise from several sources; e.g. translational motion of the sample, tilt or deformation of the electron-optical column, outer forces and vibrations, or temperature expansion. High-magnification images are very sensitive to drift distortion, since microscopic

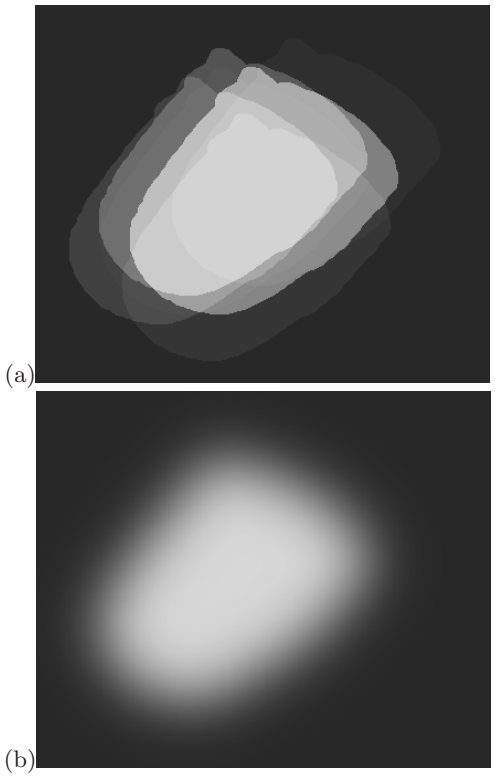

FIG. 2. Illustration of the composition (averaging) of displaced image frames. (a) Composition of a few image frames, (b) composition of a large number of frames, the image exhibits excessive blur.

displacements, tilts, or temperature changes can easily cause nanometer distortions and displacements, which can significantly impair the SEM image and its usability for nanometer-scale measurements.

The drift-distortion function is generally unknown, however, since it characterizes motion of physical bodies, it must be continuous and thus square-integrable. Therefore, drift-distortion function may be expanded to Fourier series:

$$D_{cd}(t) = \sum_{n=-\infty}^{\infty} c_n \mathrm{e}^{-\mathrm{i}nt}, \tag{6}$$

$$\vec{D}_d = \Re(D_{cd})\vec{e}_x + \Im(D_{cd})\vec{e}_y, \tag{7}$$

$$U \propto \sum_{n=-\infty}^{\infty} c_n^2 n^2, \tag{8}$$

where c_n are the (complex) Fourier coefficients, U is the overall energy of the drifting system. Since U is limited, for high n the coefficients c_n must be nearing zero. In practice, c_n for frequencies higher than 200 Hz correspond to noise only and are negligible. This approximate number is based on experimental values. Therefore, the $D_{cd}(t)$ can be written:

$$D_{cd}(t) \approx \sum_{n=-N}^{N} c_n \mathrm{e}^{-\mathrm{i}nt}, \tag{9}$$

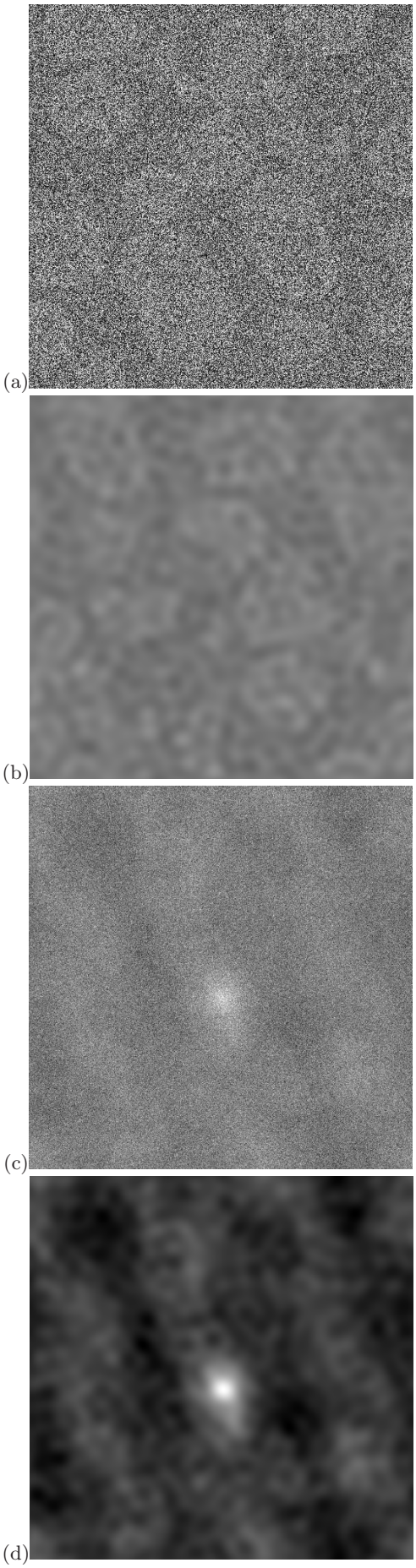

FIG. 3. Illustration of the cross-correlation displacement detection with noise filtering. (a) Original frame, (b) noise-reduced frame, (c) unprocessed cross-correlation function, and (d) correlation function of two noise-reduced frames.

where N represents the highest significant angular frequency.

SEM IMAGING METHODS

In the SEM, the acquired intensity signal always contains noise. The intensity function is thus a superposition of real signal and noise:

$$\xi(\vec{r},t) = \xi_s(\vec{r}) + \xi_n(t), \tag{10}$$

where ξ_s is the position-dependent real signal and ξ_n is the time-dependent noise. This noise is a superposition of Poisson noise, originating from the electron source and the secondary emission, noise originating from the amplifier and electronics, quantization-error noise, etc. Due to the central limit theorem, it is legitimate to suppose that the mean value of this noise is zero:

$$< \xi_n(t) >= 0. \tag{11}$$

In order to obtain a SEM image with a desired level of noise, the overall pixel dwell-time t_D must be sufficiently high. Unfortunately, the electron yield is usually low and the t_D must often be set to times ranging from tens to several hundreds of μs.

There are two common techniques to achieve this in the SEM, i.e "slow-scan" and "fast scan". With the "slow-scan" method, the image is acquired within a single scan. The acquired value is in this case:

$$I(x(t_0), y(t_0)) = \frac{K}{t_D} \int_{t_0}^{t_0+t_D} (\xi_s(\vec{r}(t)) + \xi_n(t))\, \mathrm{t}, \tag{12}$$

$$\int_{t_0}^{t_0+t_D} \xi_n(t) \mathrm{t} \approx 0, \tag{13}$$

$$\vec{r}(t) = \vec{r}_r(t_0) + \vec{D}_s(\vec{r}_r(t_0)) + \vec{D}_d(t) = \\ = \mathrm{const} + \vec{D}_d(t). \tag{14}$$

The noise is reduced by long integration as shown in Eq. (13). Required level of noise determines the dwell-time t_D. Since the desired beam position does not change during the acquisition of a single pixel, the only changing component of the position (Eq. (5)) is the D_d as stated in Eq. (14). In practice, the drift-distortion-related displacements are not significant between two pixels, because the time t_p is still not long enough. However the line-acquisition time Xt_p+t_j may already be much larger than the period of the highest frequencies. Therefore, if the "slow-scan" technique is employed, the line-scans and thus also the images may be significantly distorted (See Fig. 1). The distortion is time-dependent, and thus different for each line and image and cannot be corrected, unless additional information about the drift-distortion function $\vec{D}_d(t)$ is provided.

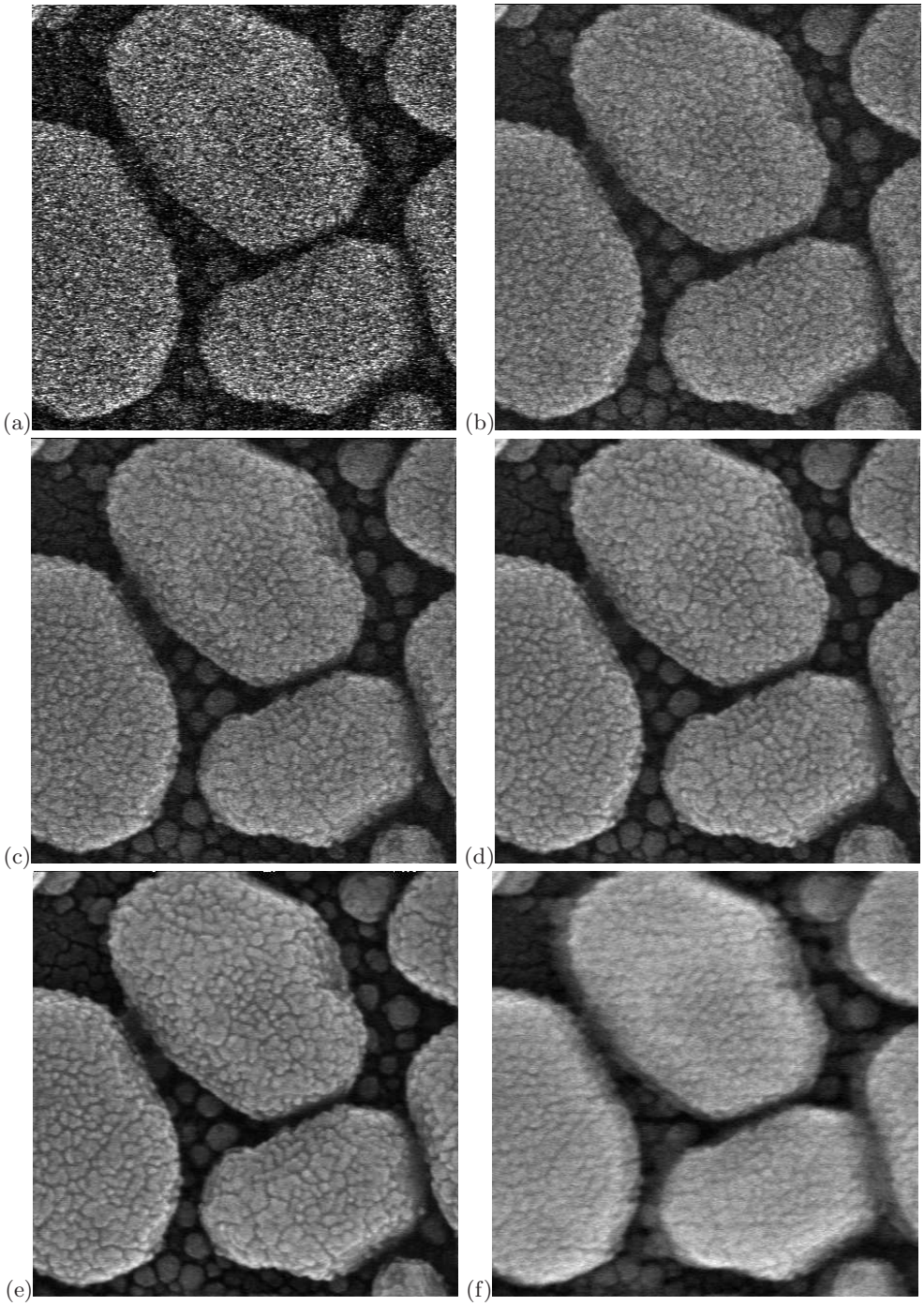

FIG. 4. Demonstration of the method on real SEM images of the gold-on-carbon resolution sample. Horizontal field-of-view is 441 nm for all images, (a) single acquired image with the pixel dwell time 50 ns, (b) composition of 10 images, (c) composition of 20 images, (d) composition of 40 images, (e) corrected composition of 120 images, and (f) Plain average of the same 120 images.

The other common imaging method in SEM is the "fast-scan". The image is composed of multiple (N_i) frames, for which averaging is the mostly applied technique. The frames are acquired with the lowest possible pixel-dwell time t_D. Since, in practice, the t_D can be set to as low as 25 ns, the change in the drift-distortion function during this time is negligible and the integral (12) can be approximated as constant. The image pixel value

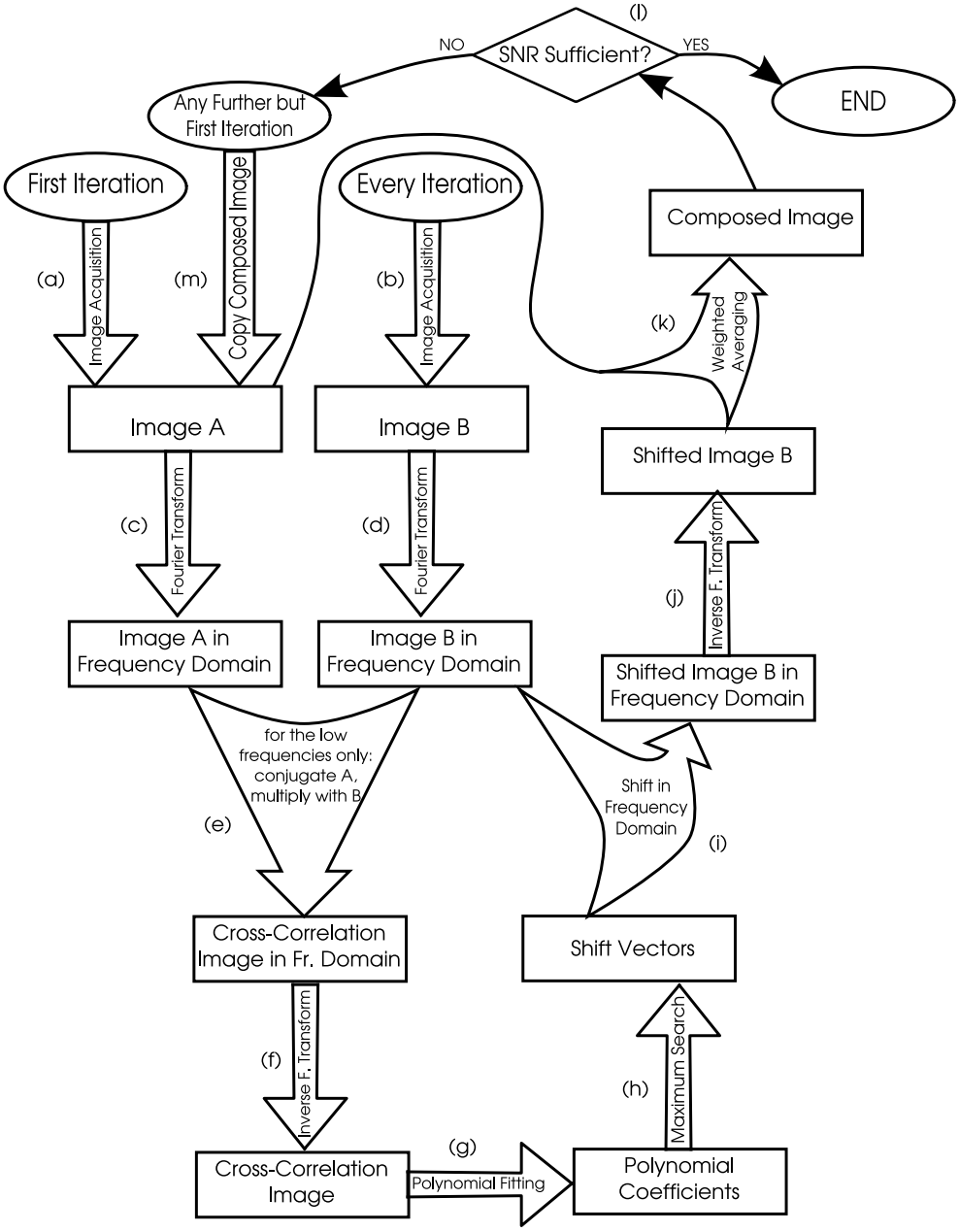

FIG. 5. Illustration of the image composition procedure. Boxes denote entities like images or numbers, arrows indicate processes. The letters (a)—(m) represent individual steps in the procedure.

is then an average of corresponding frame-pixel values:

$$I_k(x(t_0), y(t_0)) = K\xi_s(\vec{r}(t_0 + kt_f)) + \\ + K\xi_n(t_0 + kt_f), \quad (15)$$

$$I(x, y) = \frac{1}{N_i}\sum_{k=0}^{N_i} I_k(x, y). \quad (16)$$

$$t_f = Y(Xt_p + t_j) + t_{jj}, \quad (17)$$

t_f is a time period between beginnings of acquisition of two following frames, t_{jj} is the dead time between the end of acquisition of one frame and beginning of the next one.

Considering Eq. (11), the higher N_i, the lower noise level is present in the composed image. The required noise-level thus determines the number of composed frames N_i. For high N_i:

$$\sum_{k=0}^{N_i-1} \xi_n(t_0 + kt_f) \approx 0. \quad (18)$$

Because the scanning raster pattern is constant for all frames,

$$\vec{r}_r(t_0 + kt_f) = \vec{r}(t_0). \quad (19)$$

Eq. (15) may be expanded:

$$I(x(t_0), y(t_0)) = \frac{K}{N_i} \sum_{k=0}^{N_i-1} \xi_s[\vec{r}_r(t_0) + \\ + \vec{D}_s(\vec{r}_r(t_0)) + \vec{D}_d(t_0 + kt_f)]. \quad (20)$$

With current SEMs, the frame-acquisition time t_f can be much lower than the period of even the highest drift-distortion frequencies. The drift-distortion within the single-frame acquisition time is then minimal. However, it becomes significant during acquisition of the whole image, especially, when the dead times t_{jj} are high, which is the case even with many current instruments. Considering drift effects negligible within a single frame, the drift affects all image pixels equally. Point-spread function (PSF) may be constructed from the function $\vec{D}_d(t)$. Such a PSF consists of multiple separate points, which produces blurry images similar to Fig. 2. The PSF can not be used for deconvolution-based drift-distortion correction, since it is unknown like the $\vec{D}_d$ itself.

INTER-FRAME DRIFT-DISTORTION CORRECTION

The "fast-scan" method may be significantly improved using drift-distortion correction. This is possible, when the frames are taken during short enough times and $Y(Xt_p + t_j) \ll 2\pi/N$. Since the space-distortion $\vec{D}_s$ is much less pronounced and much smaller that the drift-distortion $\vec{D}_d$ at very high magnifications, it will be neglected from now on. The Eq. (20) then becomes:

$$I(x, y) = \frac{K}{N_i} \sum_{k=0}^{N_i-1} \xi_s[\vec{r}_r + \vec{D}_{dk}], \quad (21)$$

$$\vec{D}_{dk} = \vec{D}_d(t_0 + kt_f). \quad (22)$$

The image is in this case the mean value of N_i displaced images.

Fortunately, under certain conditions, it is possible to find the displacement vectors of the images, which are equal to the drift-distortion values $\vec{D}_{dk}$. These vectors then can be compensated for and thus the drift-distortion can be corrected. One possible approach is a cross-correlation-based displacement detection, which is used in this work. However, choice of the method determines the requirements, which may include low-enough noise, well-pronounced image features, etc. The complete set of requirements will be addressed in future publications.

CROSS-CORRELATION WITH NOISE REDUCTION

If two image frames f and g contain similar features at different positions, the cross-correlation integral has a large value at the vector corresponding to the displacement of the features. The SEM digital image frames are in this application represented by discrete two-dimensional real functions. Therefore, the two-dimensional discrete cross-correlation is applied.

If the image frames are noisy, the peak in the cross-correlation function becomes overridden by numerous other peaks, corresponding to random correlation of noise (Fig. 3c) This often makes finding the displacement vector impossible. This could be tackled by low-pass frequency filtering. This can be performed in the frequency domain. The cut-off frequency is determined by the filter-radius R. Although, this filter significantly wipes out all high-frequency features from the image, and therefore it is inapplicable for general reduction of noise, it still works very well for the total-maximum search of a two-dimensional function. The maximum of the cross-correlation function becomes higher above the background and it is easy to find it. (See Fig. 3d).

According to the cross-correlation theorem [7], the cross-correlation can be calculated using the Fourier transform. The widely used FFTW3 [3] algorithm is applied for Fourier transform calculations. In order to speed up the calculation, the cross-correlation is combined with the frequency filtering. (See Fig. 5e.) The conjugation and multiplication is done only in the central circle (the lowest frequencies) of the Fourier image, while the rest is zeroed:

$$J = \begin{cases} [F(f(\vec{r}))]^* \cdot F(g(\vec{r})) & \text{if } |\vec{r}| \le R, \\ 0 & \text{otherwise.} \end{cases} \quad (23)$$

$$I = F^{-1}(J) \quad (24)$$

Then, the inverse Fourier transform is applied and the noise-reduced cross-correlation image is obtained. For every pair of frames, only two forward and one inverse Fourier transforms are needed, while one of them is also part of the next pair.

SUB-PIXEL-ACCURACY DISPLACEMENT DETECTION

In order to find the displacement vectors, the maximum of the cross-correlation is searched for. Since this method is sample-dependent, there may appear problems finding the displacement vector corresponding to the transition. For example, if the image contains periodic features, there are several maxima in the cross-correlation image. In case of large blur or noise, the peak may be very wide and the uncertainty in the position of the maximum may be very high.

Plain search for maximum provides just single-pixel accuracy of the displacement-vector. The peak may be interpolated by a suitable function, which enables for calculating the displacement vectors with sub-pixel accuracy. The third-order two-dimensional polynomial function with coefficients k_0—k_9 was chosen as a suitable function for the interpolation. The coefficients may be found by polynomial fitting using the common least

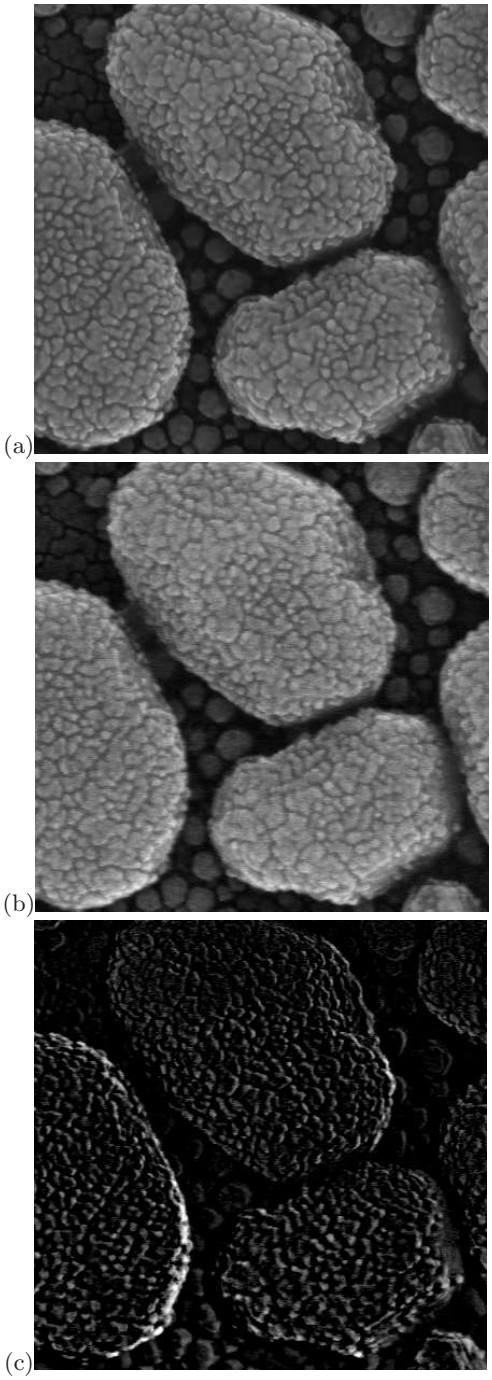

FIG. 6. The results of the corrected composition compared with the uncorrected "slow scan" demonstrated on a real SEM image of a gold-on-carbon resolution sample. Horizontal field of view is 422 nm. (a) Slow-scan image with the pixel dwell time 300 μs. (b) The result with the new technique. (c) Difference between the two images.

squares method, which is widely used in similar applications. The Cholesky factorization [4] is applied to speed the calculation. The maximum is then numerically found; its position is the searched displacement-vector with sub-pixel accuracy. However, the exact accuracy-value calculation is not covered in this article.

Since the displacement-vectors are calculated with sub-pixel accuracy, it is reasonable to shift the images with sub-pixel accuracy as well. Let the displacement-vector be $\vec{s} = s_x\vec{e}_x + s_y\vec{e}_y$. The shift can be performed with sub-pixel accuracy using the Fourier Transform, because

$$F_s(\omega, \phi) = F(\omega, \phi) \exp(-i\omega x_s - i\phi y_s). \qquad (25)$$

The obtained displacement-vectors with the sub-pixel accuracy obtained in the previous step are used for shifting, which compensates for the inter-frame drift-distortion. The corrected images are then pixel-by-pixel averaged together, however, other composition methods, e.g. median filtering, can be also used.

COMPOSITION PROCEDURE

The procedure of the method is illustrated in Fig. 5. The process starts with acquisition of two frames; A and B (Figs. 5a and b). In order to minimize the influence drift-distortion on the frames, these must be taken with minimum pixel-dwell time possible, which is usually limited by the instrument. Both frames are then converted into the frequency domain (Figs. 5c and d). These frequency-domain images are then conjugated and multiplied, which is combined with frequency filtering (Fig. 5e). This results in a cross-correlation image in the frequency domain. Then, the cross-correlation image in space domain is obtained (Fig. 5f). The cross-correlation image is interpolated by the third-order two-dimensional polynomial function. This enables finding the displacement vectors with sub-pixel accuracy (Fig. 5g). The coordinates of the maximum denote the found displacement vector (Fig. 5h). This displacement vector is used to shift the image B in its frequency-domain representation, which enables the sub-pixel accuracy alignment (Fig. 5i). Shifted image B is converted into the space domain (Fig. 5j) and averaged with the image A (Fig. 5k). Image A has (except in the first iteration) higher information weight, as it already represents a sum of multiple image frames. If the SNR is not sufficient (Fig. 5l), the composed image is copied into the frame A (Fig. 5m) and a new frame B is acquired. The process then repeats until the SNR is sufficient, or the software runs out of frames.

RESULTS

The discussed image-composition method was tested on gold-on-carbon resolution images (Fig. 4) and on artificial images. A Mac Pro computer with two dual-core Intel Xeon Central Processor Units (CPUs) and 4 GB of Random Access Memory (RAM) was employed for the calculations. The 64-bit edition of Gentoo Linux Operating System (OS) was installed on the computer.

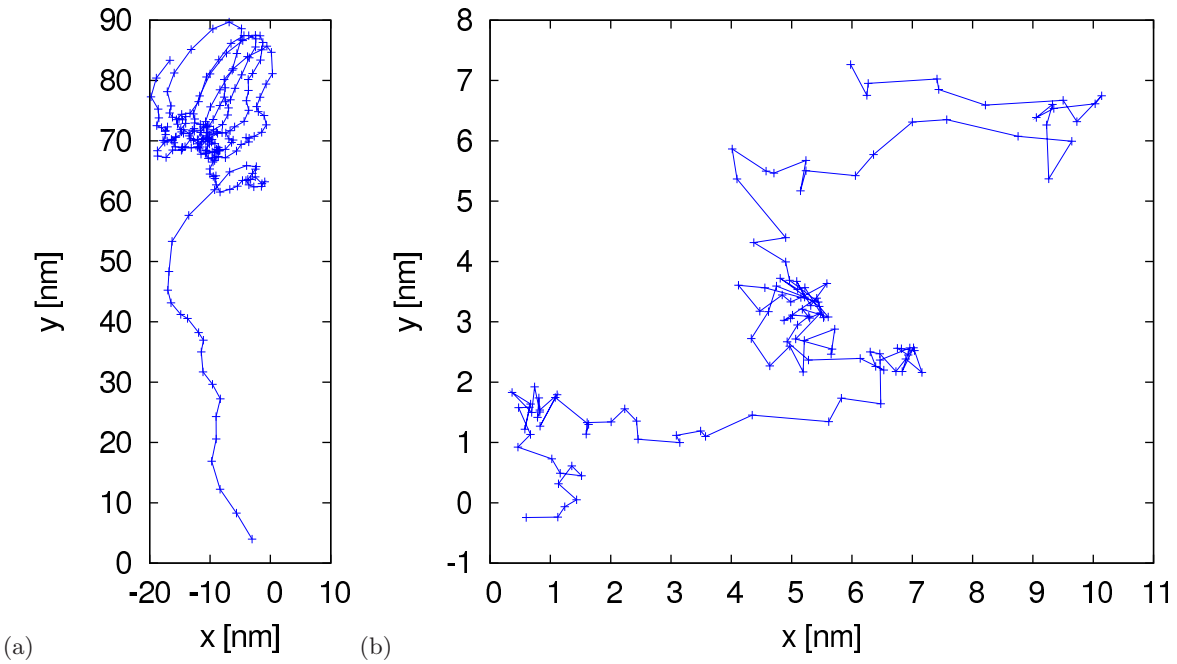

FIG. 7. Example of a drift tracking. Subsequent displacement vectors are displayed in the graph. (a) Drift-distortion of a sample placed on a fixed stage. Frames were taken every 60 s. (b) Drift distortion of the sample used in Fig. 4. Frames were taken every 1 s.

For the real images, the pixel dwell time was set to the lowest instrument setting (50 ns). The frame-rate was 1 frame per second, which was also the fastest setting. Single acquired frame (Fig. 4a) was very noisy; only the most prominent features (about 200 nm in diameter) were clearly visible. A composition of 10 frames (Fig. 4b) already contained visible features in the background (about 20 nm in diameter); some inner structure of the grains (sized about 5-10 nm) became observable. Compositions of 20 (Fig. 4c) and 40 (Fig. 4d) frames embodied some more detail. The inner structure of the grains, as well as all the background features are clearly visible. The composition of 120 frames from the new composition method (Fig. 4e) and the existing averaging method (Fig. 4f) are included for a comparison of the new and the traditional averaging methods. The traditionally averaged image was significantly more blurred than the image composed using the described method. Both images have similar SNR. The final image (Fig. 4e) exhibits low noise and high detail whilst preserving the shapes and dimensions.

The slow-scan image is displayed in Fig. 6a. The pixel dwell time was 300 μs, which is a common choice for such imaging. The image looked clean and noise free on inspection; however, the difference between the slow-scan image and the image obtained with the new composition method, as shown in Fig. 6c exhibited a significant difference, which is believed to be associated with the distortions in the slow-scan image. The image was acquired for 6000 times longer time than the image in Fig. 4a and the drift-distortion affected the shapes significantly.

The obtained sequences of displacement-vectors were also used to track the sample position with respect to the beam (Fig. 7). This information was very usable for drift investigation. In the case of the sample of the fixed stage, displayed in Fig. 7a, there was a roughly 70-nm-long straight start-up drift followed by a periodical circular drift, which was caused by periodical temperature changes inside the electron-optical column.

On the other hand, the Fig. 7b shows the displacement-vector sequence associated with a typical drift in the SEM. Assuming the obtained curve to be associated with a relative trajectory of physical bodies with a position noise superimposed to it, it is possible to estimate the accuracy of the displacement-vector searching to be approximately 0.5 nm, which corresponds to 0.5 pixels.

Speed of calculation is another important aspect of this method and its implementation. It was not possible to try the technique in a real-time imaging application, since this would require integration of the technique into the SEM software, which was not possible. However, the calculation times were measured and on 512×512-pixel-large images, a single search for a displacement-vector took in average 0.08 s, while the times of individual frame compositions are very consistent.

CONCLUSION

The technique is implemented as a computer program written in C language, which is the advantage due to its optimization possibilities and ease of possible incorpora-

tion into SEM software. On reasonably fast computers, this program is capable of real-time processing. The algorithm is well distributable, thus, it is suitable for running on computer clusters or multi-core or multi-processor environments, including graphics processing units (GPUs). The method has been verified on real and artificial SEM images demonstrating its usability for true-shape imaging and for drift investigation applications. It was also tested for the calculation speed, which is high enough for real-time processing, when integrated into the SEM software.

Since the power of this method strongly depends on many factors, e.g. sample-feature shapes, noise, image size, etc., its limits should be throughly examined. Calculation of accuracy and confidence intervals, influence of sample charging and contamination are still under investigation. These issues will be addressed in future works on this project.

[1] S. Chang, C. S. Wang, C. Y. Xiong, and J. Fang. Nanoscale in-plane displacement evaluation by AFM scanning and digital image correlation processing. *Nanotechnology*, 16(4):344–349, APR 2005.

[2] P. Cizmar, A. E. Vladar, B. Ming, and M. T. Postek. Simulated SEM Images for Resolution Measurement. *Scanning*, 30(5):381–391, Sep-Oct 2008.

[3] M. Frigo and S. G. Johnson. The design and implementation of FFTW3. In *Proceedings of the IEEE*, volume 93, pages 216–231, FEB 2005.

[4] J. E. Gentle. *Numerical Linear Algebra for Applications in Statistics*. Springer-Verlag, Berlin, 1998.

[5] T. Kawasaki, H. Utsuro, Y. Takai, and R. Shimizu. Evaluation of image drift correction by three-dimensional Fourier analysis. *Journal of Electron Microscopy*, 48(1):35–37, 1999.

[6] B. A. Mantooth, Z. J. Donhauser, K. F. Kelly, and P. S. Weiss. Cross-correlation image tracking for drift correction and adsorbate analysis. *Review of Scientific Instruments*, 73(2, Part 1):313–317, FEB 2002.

[7] A. Papoulis. *The Fourier integral and its applications*. Mc Graw-Hill, New York, 1962.

[8] M. T. Postek, J. S. Villarrubia, and A. E. Vladar. Advanced electron microscopy needs for nanotechnology and nanomanufacturing. *Journal of Vacuum Science & Technology B*, 23(6):3015–3022, NOV-DEC 2005.

[9] M. T. Postek, A. E. Vladar, M. H. Bennett, T. Rice, and R. Knowles. Photomask dimensional metrology in the scanning electron microscope, part II: High-pressure/environmental scanning electron microscope. *Journal of Microlithography Microfabrication and Microsystems*, 3(2):224–231, APR 2004.

[10] M. A. Sutton, N. Li, D. Garcia, N. Cornille, J. J. Orteu, S. R. McNeill, H. W. Schreier, and X. Li. Metrology in a scanning electron microscope: theoretical developments and experimental validation. *MEASUREMENT SCIENCE & TECHNOLOGY*, 17(10):2613–2622, OCT 2006.

[11] M. A. Sutton, N. Li, D. Garcia, N. Cornille, J. J. Orteu, S. R. McNeill, H. W. Schreier, X. Li, and A. P. Reynolds. Scanning electron microscopy for quantitative small and large deformation measurements - part II: Experimental validation for magnifications from 200 to 10,000. *EXPERIMENTAL MECHANICS*, 47(6):789–804, DEC 2007.

[12] M. A. Sutton, N. Li, D. C. Joy, A. P. Reynolds, and X. Li. Scanning electron microscopy for quantitative small and large deformation measurements part I: SEM imaging at magnifications from 200 to 10,000. *EXPERIMENTAL MECHANICS*, 47(6):775–787, DEC 2007.

[13] Z-H Xu, X-D Li, M. A. Sutton, and N. Li. Drift and spatial distortion elimination in atomic force microscopy images by the digital image correlation technique. *Journal of Strain Analysis for Engineering Design*, 43(8, Sp. Iss. SI):729–743, NOV 2008.